The effect of buffer-layer on the steady-state energy release rate of a tunneling crack in a wind turbine blade joint

Jørgensen, Jeppe Bjørn; Sørensen, Bent F.; Kildegaard, Casper

Published in:
Composite Structures

Link to article, DOI:
10.1016/j.compstruct.2017.12.081

Publication date:
2018

Document Version
Peer reviewed version

The effect of buffer-layer on the steady-state energy release rate of a tunneling crack in a wind turbine blade joint

Jeppe B. Jørgensen[a,b,*], Bent F. Sørensen[b], Casper Kildegaard[a]

[a] *LM Wind Power, Østre Alle 1, 6640 Lunderskov, Denmark.*
[b] *The Technical University of Denmark, Dept. of Wind Energy, Frederiksborgvej 399, 4000 Roskilde, Denmark.*

Abstract

The effect of a buffer-layer on the steady-state energy release rate of a tunneling crack in the adhesive layer of a wind turbine blade joint, loaded in tension, is investigated using a parametric 2D tri-material finite element model. The idea of embedding a buffer-layer in-between the adhesive and the basis glass fiber laminate to improve the existing joint design is novel, but the implications hereof need to be addressed.

The results show that it is advantageous to embed a buffer-layer near the adhesive with controllable thickness- and stiffness properties in order to improve the joint design against propagation of tunneling cracks. However, for wind turbine blade relevant material combinations it is found more effective to reduce the thickness of the adhesive layer since the stiffness mismatch between the existing laminate and the adhesive is already high. The effect of material orthotropy was found to be relatively small for the blade relevant materials.

Keywords: Tunneling crack, Adhesive bonded joints, Fracture mechanics, Polymer matrix composites, Finite element analysis

Nomenclature

E_1	Young's modulus of substrate
E_2	Young's modulus of adhesive
E_3	Young's modulus of buffer-layer
$\bar{E}_1$	plane strain Young's modulus of substrate
$\bar{E}_2$	plane strain Young's modulus of adhesive

*Corresponding author
Email address: jbj@lmwindpower.com (Jeppe B. Jørgensen)

$\bar{E_3}$	plane strain Young's modulus of buffer-layer
F	non-dimensional function
$\mathcal{G}_{ss}$	mode-I steady-state energy release rate
G_{xy}	shear modulus
h_1	thickness of substrate
h_2	half thickness of the adhesive layer
h_3	thickness of buffer-layer
x, y, z	coordinates
α_{12}	first Dundurs' parameter (substrate/adhesive)
α_{32}	first Dundurs' parameter (buffer-layer/adhesive)
β_{12}	second Dundurs' parameter (substrate/adhesive)
β_{32}	second Dundurs' parameter (buffer-layer/adhesive)
δ_{cod}	crack opening displacement profile
λ	first orthotropy parameter
ν	Poisson's ratio
ρ	second orthotropy parameter
$\sigma_{yy,2}$	stress in the adhesive (y-direction)
Biax	bi-axial
FE	finite element
UD	uni-directional

1. Introduction

A typical wind turbine blade joint is manufactured of a structural adhesive layer that is bonding two glass fiber laminated shells meaning that the structural adhesive is constrained in-between stiffer laminates. This is exemplified in Figure 1 (A) for a trailing-edge joint in a wind turbine blade. Observations from full scale blade tests of this joint with tensile stresses, $\sigma_{yy,2}$, in the adhesive, show that cracks can initiate at the free-edge and propagate through the adhesive layer as a so-called tunneling crack. The tunneling crack is constrained by the laminates as shown in the sketch in Figure 1 (A) and the photo in Figure 1 (B).

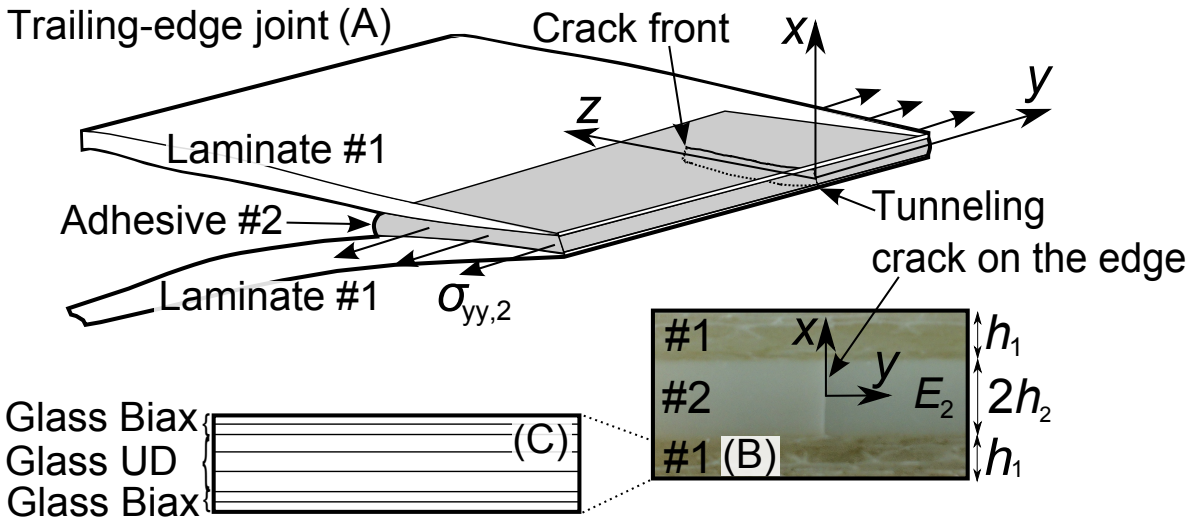

Figure 1: (A) Trailing-edge joint with a tunneling crack propagating across the adhesive layer in the z-direction. (B) Photo of a tunneling crack in a trailing-edge wind turbine blade joint. (C) Typical layers in a glass fiber laminate used in a wind turbine blade joint.

Novel models are desired for establishing design rules for an improved joint design in order to prevent tunneling cracks propagating across the wind turbine blade joint in Figure 1 (A). An improved joint design aims at decreasing the energy release rate for tunneling cracks in the joint and thus enable a reduction in the amount of reinforcement needed in the laminates. This leads to a reduction in blade mass and thus a decrease in the cost of energy since lighter blades are more efficient and can save structural reinforcement in the other wind turbine components e.g. nacelle, hub, tower and foundation [1].

Generally, the process of tunneling crack propagation includes three-dimensional effects. However, when the crack in Figure 1 (A) reaches a certain length from the edge (in z-direction), the energy release rate becomes steady-state meaning that the energy release rate no longer depends on the crack length. The problem of steady-state propagation of a tunneling crack was analysed for an isotropic bi-material model by Ho and Suo [2, 3]. Although tunneling cracking is a 3D problem, the steady-state energy release rate, can be determined exact from a 2D solution by [2, 3]:

$$\mathcal{G}_{ss} = \frac{1}{2}\frac{\sigma_{yy,2}}{2h_2}\int_{-h_2}^{+h_2}\delta_{cod}(x)dx \tag{1}$$

where $\sigma_{yy,2}$ is the far field stress in the cracked adhesive layer (uniform applied stress) and the adhesive thickness is $2h_2$ according to Figure 1. $\delta_{cod}(x)$ is the crack opening displacement profile for the plane strain crack far behind the crack front. For the elementary case of a central crack in an infinitely large plate subjected to remote tensile stresses (Griffith crack), the crack opening displacement is [3]:

$$\delta_{cod} = \frac{4\sigma_{yy,2}}{\bar{E}_2}\sqrt{(h_2^2 - x^2)} \tag{2}$$

where $\bar{E}_2$ is the plane strain Young's modulus of the plate. Inserting equation 2 into equation 1 and evaluating the integral gives [2, 3]:

$$\mathcal{G}_{ss} = \frac{\pi}{4}\frac{\sigma_{yy,2}^2 2h_2}{\bar{E}_2} \qquad \textit{(asymptotic limit)} \tag{3}$$

This asymptotic limit, established by Ho and Suo [2, 3] in equation 3, is representing the mode-I steady-state energy release rate of a tunneling crack in a homogenous structure with infinitely thick substrates. Therefore, it is convenient to normalise other energy release rate results with this elementary case i.e. $[(\sigma_{yy,2}^2 2h_2)/(\bar{E}_2)]$.

The tunneling crack models by Ho and Suo [2, 3] were extended to account for debonding [4, 5, 6], transient effects for short crack lengths [7] (although first demonstrated for thin film [8, 9]) and material orthotropy [10, 11]. Yang *et al.* [10] studied the effect of ply angles on the critical stress to propagate a tunneling crack embedded in the central layer of a carbon-epoxy laminate. It was found that the critical stress to propagate the tunneling crack were highest when the uni-directional fibers were oriented perpendicular to the tunneling crack i.e. fibers oriented in the y-direction in Figure 1. Beom *et al.* [11] presented results for the case where only the adhesive layer was modelled with material orthotropy i.e. the modelling results were limited to substrates with isotropic material properties of infinitely thickness.

In a wind turbine blade joint the adhesive can be assumed isotropic, but the substrates consist of several layers of different type, typically uni-directional- (UD) and bi-axial (Biax) glass-fiber layers as exemplified in Figure 1 (B-C). The in-plane orthotropy of these materials can be described by two dimensionless parameters [12]:

$$\lambda = \frac{E_{xx}}{E_{yy}}, \qquad \rho = \frac{(E_{xx}E_{yy})^{1/2}}{2G_{xy}} - (\nu_{xy}\nu_{yx})^{1/2} \tag{4}$$

which reduces to $\lambda = \rho = 1$ for an isotropic material [12]. The material directions of the laminate are in accordance with the coordinate system in Figure 1, where E_{xx} and E_{yy} are the Young's modulus, G_{xy} is the shear modulus, and ν_{xy} and ν_{yx} are the Poisson's ratio.

The substrates, constraining the adhesive, can be modified in order to prevent the propagation of tunneling cracks since the substrates are layered composite materials. Thus, one way of improving the adhesive joint design is to modify the ply-thickness and stiffness of the individual layers of the laminates. However, modification of the original layup might have a negative effect on the existing blade design that is designed such that the joint can withstand the various other load cases e.g. bending, compression and torsion.

Another way to prevent tunneling crack propagation across the adhesive layer of the joint is to add a new layer, called a buffer-layer, near the adhesive and control the properties of this layer. The buffer-layer design philosophy is attractive since the original joint design can be maintained and at

the same time, by adding the buffer-layer, the joint design can be improved against the propagation of tunneling cracks. Furthermore, it is well known for thin films that it is the thickness and stiffness of the layer closest to the adhesive that has the greatest constraining effect on the crack [13].

The objective of this research is to study the effect of in-plane stiffness, E, and layer-thickness, h, on the steady-state energy release rate, $\mathcal{G}_{ss}$, using finite element (FE) models. More specifically, it is the aim to determine the effect of a buffer-layer on the steady-state energy release rate for an isolated tunneling crack in the adhesive layer of a wind turbine blade joint. This should lead to design rules for an improved bonded joint design. The primary applicability is for wind turbine blade relevant joint design and -material combinations since there is a high demand for novel design rules for adhesive joints in the wind turbine blade industry.

The design idea of a buffer-layer for improvement of a wind turbine blade joint is novel and the implications and effects of this buffer-layer need to be investigated before potential implementation in the future joint design. Therefore, parameter studies with a new symmetric tri-material FE model is used to address the design challenge. Furthermore, the study of steady-state tunnel cracking for a multi-layered sandwich structure with orthotropic substrates has not been addressed in the literature. This includes the applicability on wind turbine blade joints with realistic material combinations.

The paper is organised as follows. In section 2 the materials and the problem are defined, and in section 3 the finite element modelling techniques are described. Hereafter, tunneling cracking in a generalised perspective is analysed using first bi-material FE models in section 4 and tri-material FE models in section 5 (see Figure 2). In section 6, a case study with blade relevant materials demonstrates how a wind turbine blade joint design are influenced by the presence of a buffer-layer including the effect of material orthotropy. Finally, a discussion and conclusion highlights the major findings of the present study.

2. Problem definition

The problem we investigate in the present study is that of an isolated tunneling crack in Figure 2 (A), which is used to clarify the effect of substrate stiffness- and thickness, and used to test the implementation of the numerical models. This model is extended by embedding a buffer-layer, named material #3 in Figure 2 (B), to analyse the effect of buffer-layer thickness and -stiffness on the steady-state energy release rate of a tunneling crack. The model is limited to three layers since more layers complicate the modelling unnecessarily. The effect of material orthotropy of the substrates is investigated in order to test whether it is feasible to model blade relevant materials as isotropic materials.

Since stress is applied as boundary condition in the tunneling crack models, Dundurs' parameters

can be introduced to reduce the number of elastic parameters controlling the stress field [14, 15]:

$$\alpha_{i2} = \frac{\bar{E}_i - \bar{E}_2}{\bar{E}_i + \bar{E}_2} \qquad and \qquad \beta_{i2} = \frac{\bar{E}_i f(\nu_2) - \bar{E}_2 f(\nu_i)}{\bar{E}_i + \bar{E}_2} \tag{5}$$

For the bi-material model in Figure 2 (A), $i = 1$ represents the substrate and for the tri-material model in Figure 2 (B), $i = 1, 3$ denotes the substrate and buffer-layer respectively. ν_i is Poisson's ratio and E_i is the in-plane Young's modulus. $\bar{E}_i = E_i/(1-\nu_i^2)$ and $f(\nu_i) = (1-2\nu_i)/[2(1-\nu_i)]$ are for plane strain, and $\bar{E}_i = E_i$ and $f(\nu_i) = (1-2\nu_i)/2$ are for plane stress. The Young's modulus of the UD composite in the fiber direction, E_{yy}, is used for the computation of α for the orthotropic materials. $\bar{E}_2$ is the plane strain Young's modulus of the adhesive.

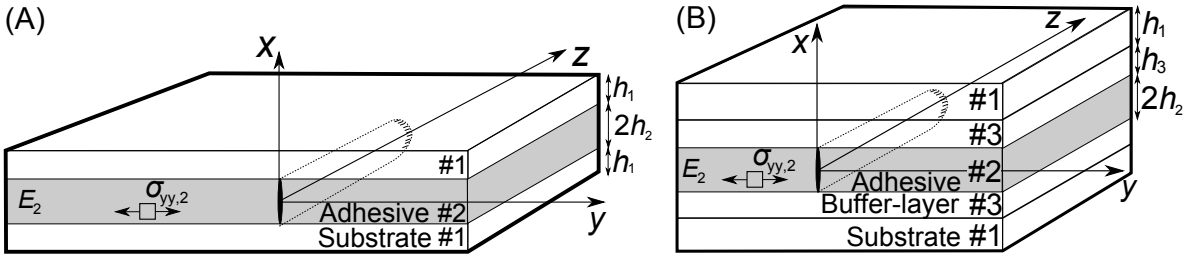

Figure 2: (A) Bi-material model. (B) Tri-material model.

The primary stiffness of a bi-axial glass fiber laminate (Glass Biax), a uni-directional glass fiber laminate (Glass UD) and a uni-directional carbon-fiber laminate (Carbon UD) are used in the present study. These materials, referred to as "blade relevant materials", are modelled as both isotropic and orthotropic with the material parameters presented in Table 1. The constitutive properties of Glass UD and Glass Biax laminates are comparable to those presented by Leong *et al.* [16], whereas for the Carbon UD laminate the properties are close to those of the carbon-epoxy laminate used by Yang *et al.* [10]. The in-plane stiffness, E_{yy}, for Glass UD and Carbon UD are also comparable to the values used in the wind turbine blade design by Mikkelsen [17]. For the cases with isotropic materials ($\lambda = \rho = 1$), the Young's modulus of the substrate, E_1, is set equal to the Young's modulus of a UD composite in the fiber direction, E_{yy}, since this is the primary stiffness parameter constraining the crack. For all models the adhesive is modelled as isotropic and $\nu_i = 1/3$ such that for plane strain $\beta_{i2} = \alpha_{i2}/4$.

	Isotropic				Orthotropic			
Material name	α_{i2}	β_{i2}	λ	ρ	α_{i2}	β_{i2}	λ	ρ
Glass Biax	0.54	0.13	1.00	1.00	0.54	0.13	1.00	0.67
Glass UD	0.85	0.21	1.00	1.00	0.85	0.21	0.26	1.62
Carbon UD	0.94	0.23	1.00	1.00	0.94	0.23	0.11	2.69

Table 1: Material properties for "blade relevant materials".

3. Finite element modelling of a tunneling crack

In the present study $\delta_{cod}(x)$ in equation 1 is determined by a 2D FE model with eight-noded plane strain elements simulated in Abaqus CAE 6.14 (Dassault Systemes). Numerical integration is used to evaluate the integral in equation 1. The steady-state energy release rate, $\mathcal{G}_{ss}$, for the tunneling crack in the bi-material structure, shown in Figure 2 (A), is determined by:

$$\frac{\bar{E}_2 \mathcal{G}_{ss}}{\sigma_{yy,2}^2 2h_2} = F(\alpha_{12}, \beta_{12}, h_1/h_2) \tag{6}$$

where $F(\alpha_{12}, \beta_{12}, h_1/h_2)$ is a non-dimensional function, determined numerically, that accounts for the stiffness mismatch and geometry [2]. The steady-state energy release rate for the tunneling crack in the tri-material structure, shown in Figure 2 (B), can be written as:

$$\frac{\bar{E}_2 \mathcal{G}_{ss}}{\sigma_{yy,2}^2 2h_2} = F(\alpha_{12}, \alpha_{32}, \beta_{12}, \beta_{32}, h_1/h_2, h_3/h_2) \tag{7}$$

where again the non-dimensional function, F, is determined numerically. For both the bi- and tri-material models, the smallest element side length is $0.025h_2$ and approximately 80 elements (eight-noded plane strain) are used across the thickness of the adhesive.

4. Results from tunneling crack bi-material FE model

Figure 3 (B) shows finite element results; $F(\alpha_{12}, \beta_{12} = \alpha_{12}/4, h_1/h_2)$ decreases with increasing substrate stiffness and -thickness. Comparing the FE results for $h_1/h_2 = 2.0$ with the results by Ho and Suo [2] shows that the maximum deviation is below 2%, which indicates that the numerical implementation is sufficiently accurate. The maximum deviation is identified for very compliant substrates. For $\alpha_{12} = 0.0$ in Figure 3 (A), the deviation between the numerical solution and the *asymptotic limit* (Ho and Suo [2]) of $\pi/4$ in equation 3 is less than 0.3% when $h_1/h_2 \geq 6.0$. Furthermore, Figure 3 (A) shows that for decreasing elastic mismatch, α_{12}, the larger h_1/h_2 must be for $\mathcal{G}_{ss}$ to reach a constant value. In Figure 3 (B) an approximate asymptotic limit is identified; when $\alpha_{12} \to 1.0$ and $h_1/h_2 \to \infty$ then $F(\alpha_{12}, \beta_{12} = \alpha_{12}/4, h_1/h_2) \approx 1/2$.

Figure 4 shows the effect of increasing substrate thickness on $F(\alpha_{12}, \beta_{12} = \alpha_{12}/4, h_1/h_2)$ for blade relevant materials. For all types of substrates, where the stiffness of the blade relevant materials are relatively high in comparison with the adhesive, $F(\alpha_{12}, \beta_{12} = \alpha_{12}/4, h_1/h_2)$ starts high, decays and approaches a steady level when $h_1/h_2 \geq 4.0$, see Figure 4. The maximum relative deviation between the models with isotropic- and orthotropic material properties in Figure 4 are 1.9%, 6.0% and 7.2% for Glass Biax, Glass UD and Carbon UD, respectively.

For orthotropic Glass Biax (for which $\rho < 1.0$ i.e. the shear modulus, G_{xy}, is larger for the orthotropic material than for the corresponding isotropic material) the curve in Figure 4 is slightly

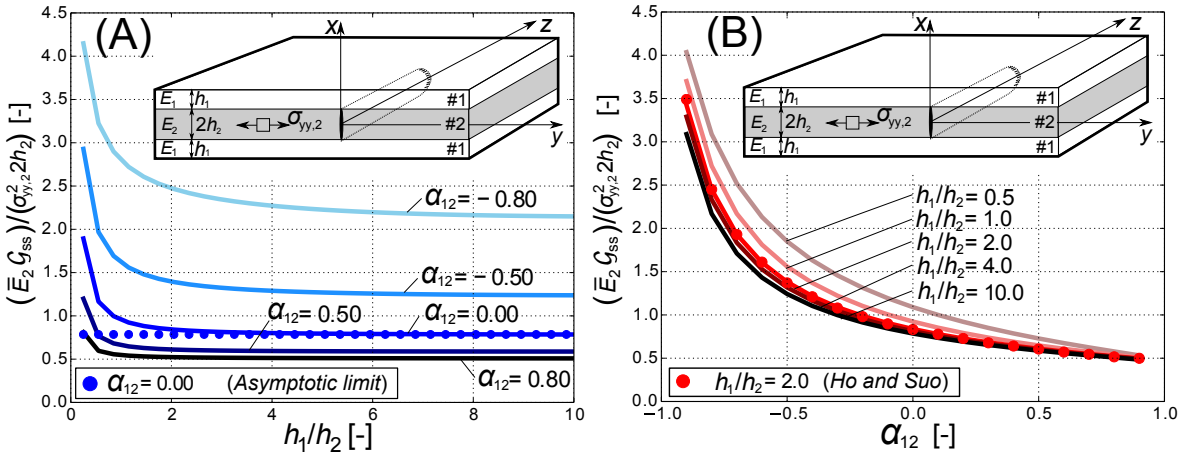

Figure 3: Steady-state energy release rate results for different h_1/h_2 and α_{12}: (A) from bi-material FE model compared with the asymptotic limit ($\pi/4$) from Ho and Suo [2] that is valid for infinitely thick substrates. (B) from bi-material FE model compared with the results by Ho and Suo [2]. Note, for both models $\beta_{12} = \alpha_{12}/4$.

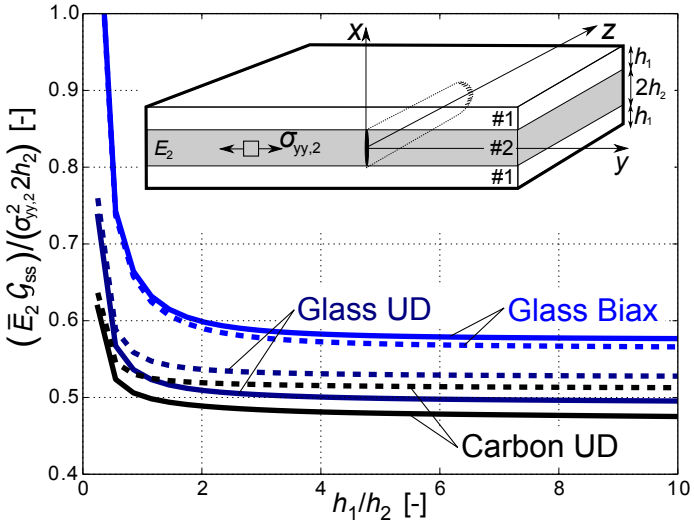

Figure 4: Steady-state energy release rate results from a bi-material FE model for "blade relevant materials" for different stiffness mismatch and with $\beta_{12} = \alpha_{12}/4$. Solid lines and dashed lines represent isotropic- and orthotropic material properties, respectively.

below the curve of the isotropic material. For Glass UD and Carbon UD where $\rho > 1.0$, the energy release rate is higher for the orthotropic case than for the isotropic case.

5. Results from tri-material FE model - generalised joint design

Figure 5 illustrates the influence of buffer-layer thickness and -stiffness on $\mathcal{G}_{ss}$ when $h_1/h_2 = 1.0$. For all cases in Figure 5 it is evident that an increase in α_{32} decreases $\mathcal{G}_{ss}$. It is seen that an increase of buffer-layer thickness, h_3/h_2, decreases $\mathcal{G}_{ss}$ if $\alpha_{32} \gtrsim \alpha_{12}$. Note, that the limit values indicated by arrows in Figure 5 are determined using the bi-material FE model at $h_3/h_2 = 10$. These limit values are identical to the results from the bi-material FE model in Figure 3 at $h_1/h_2 = 10$ indicating that for high buffer-layer thickness, the buffer-layer is the primary layer controlling $\mathcal{G}_{ss}$ (not the substrate).

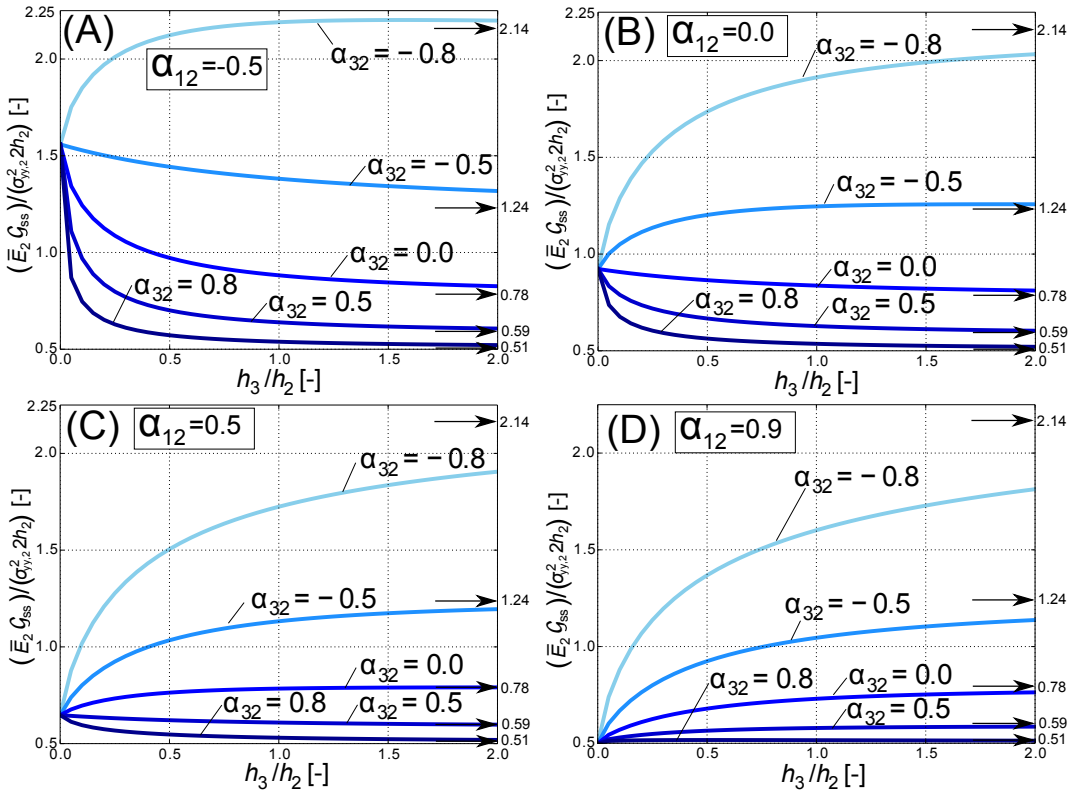

Figure 5: Steady-state energy release rate results from a symmetric tri-material FE model with isotropic materials and selected parameters fixed: $\beta_{i2} = \alpha_{i2}/4$, $h_1/h_2 = 1.0$. Substrate stiffness mismatch of: (A) $\alpha_{12} = -0.5$, (B) $\alpha_{12} = 0.0$, (C) $\alpha_{12} = 0.5$ and (D) $\alpha_{12} = 0.9$.

Further design curves are presented in Figure 6 where α_{32} is varied for different h_3/h_2 and α_{12}. The design curves in Figure 6 for each stiffness mismatch, α_{12}, intersect at a specific point, namely the "point of intersection" (PoI) that is marked with "X" in Figure 6. On the right hand side of the "point of intersection" ($\alpha_{32} >$ PoI), it is advantageous to increase the buffer-layer thickness, whereas on the

left hand side of the "point of intersection" ($\alpha_{32} <$ PoI), it is advantageous to decrease the buffer-layer thickness. It is also evident from Figure 6 that with increasing α_{12} the "point of intersection" moves to the right (to a larger α_{32} value).

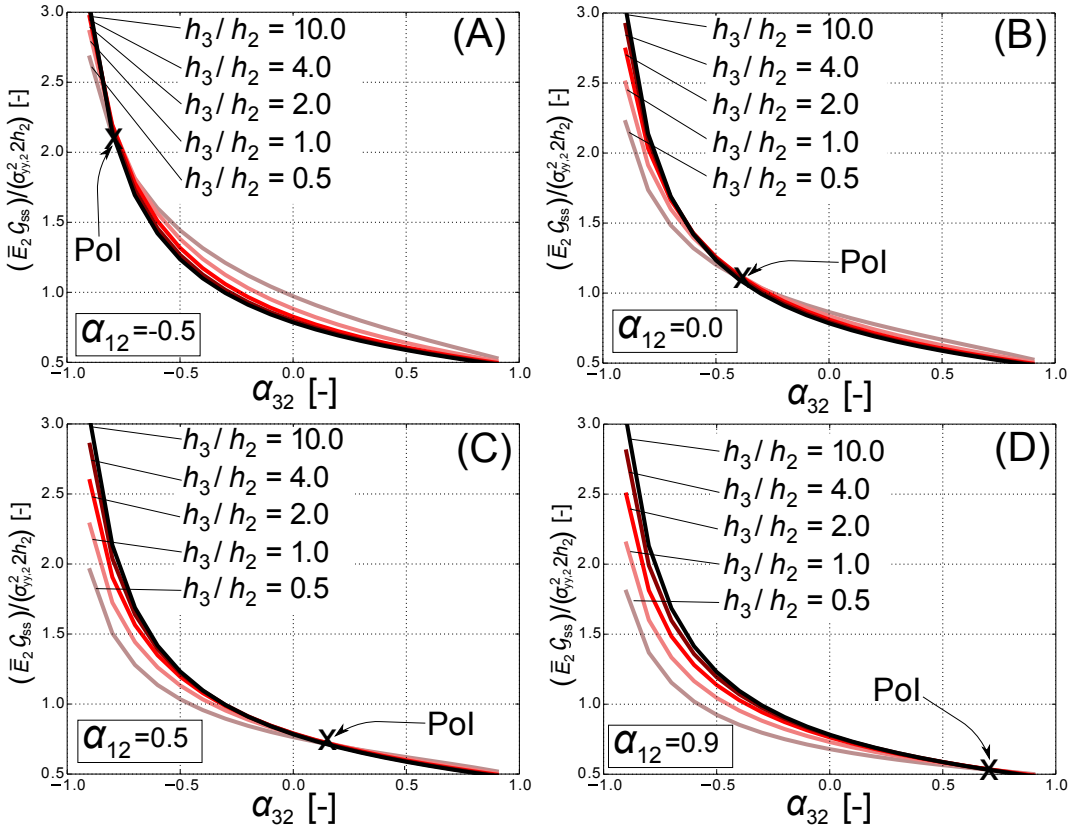

Figure 6: Steady-state energy release rate results from a symmetric tri-material FE model with isotropic materials and selected parameters fixed: $\beta_{i2} = \alpha_{i2}/4$, $h_1/h_2 = 1.0$. Substrate stiffness mismatch of: (A) $\alpha_{12} = -0.5$, (B) $\alpha_{12} = 0.0$, (C) $\alpha_{12} = 0.5$ and (D) $\alpha_{12} = 0.9$.

The best choice (i.e. the one that gives the lowest energy-release rate) of buffer-layer thickness and stiffness depends on the stiffness of the basis substrate, α_{12}. Without prior knowledge of the modeling result it would be expected that the stiffness of the buffer-layer should be a least the stiffness of the substrate in order to reduce the energy release rate. However, the value of α_{32} at the "point of intersection" is less than the value of α_{12} in the models in Figure 6. For instance, it is seen in Figure 6 (C) that the PoI is located at $\alpha_{32} \approx 0.25$, whereas $\alpha_{12} = 0.5$ for the model in Figure 6 (C). Thus, the "point of intersection" must be determined accurately in order to ensure that $\mathcal{G}_{ss}$ decreases with increasing h_3/h_2. An additional study of the transition at the "point of intersection" is presented in Appendix A. In the overall picture, changing the stiffness of the basis substrate (α_{12}) has a small effect on the steady-state energy release rate of the tunneling crack.

6. Results for case study with blade relevant materials

The parametric 2D plane strain FE model of an isolated tunneling crack with a buffer-layer, denoted material #3 in Figure 7, is used to investigate the effect of buffer-layer thickness and -stiffness on $\mathcal{G}_{ss}$ for blade relevant material combinations including the effect of material orthotropy. The stiffness of the substrate (material #1) is equal to that of Glass UD ($\alpha_{12} = 0.85$).

First the results for the case where the stiffness of the buffer-layer (material #3) is similar to that of Glass Biax ($\alpha_{32} = 0.54$) is presented. The curves in Figure 7 for Glass Biax shows that an increase of the buffer-layer thickness, h_3, actually increases $\mathcal{G}_{ss}$ although the total thickness of the substrate ($h_1 + h_3$) becomes larger. This can be understood in that with increasing h_3, the stiffer material #1 is moved further away from the tunneling crack tip hence reducing the constraint, but also by the decreased stiffness of the layer closest to the adhesive.

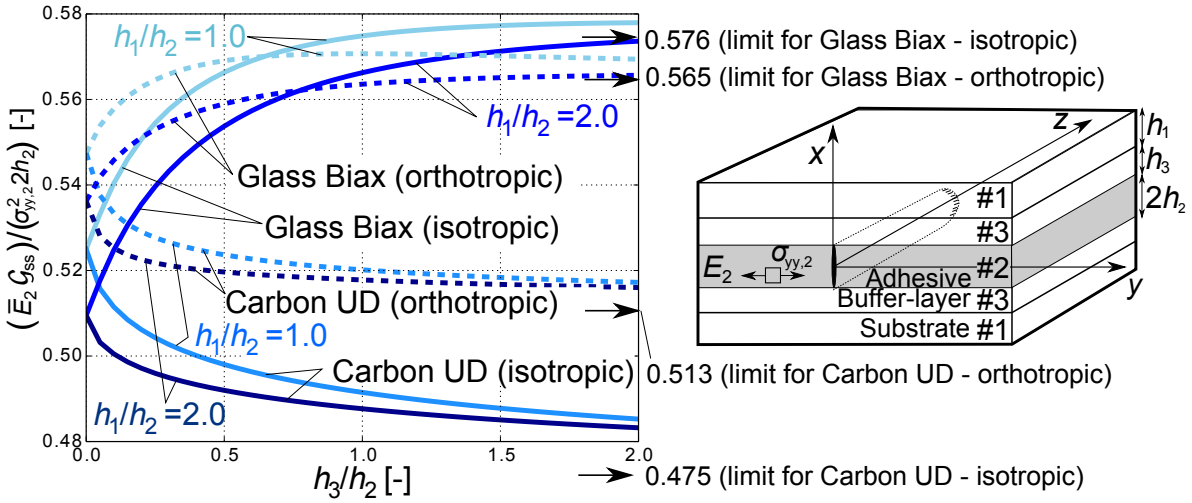

Figure 7: Steady-state energy release rate results from a symmetric tri-material FE model with blade relevant material combinations. Solid lines and dashed lines represent isotropic- and orthotropic material properties, respectively. The limit values indicated by arrows are determined using the results of the bi-material FE model at $h_3/h_2 = 10$ in Figure 4.

Figure 7 also includes results for a buffer-layer with stiffness of a Carbon UD laminate ($\alpha_{32} = 0.94$). The thickness, h_3, of material #3 is varied and the results show that a design for reducing $\mathcal{G}_{ss}$ would consist of a thick and stiff layer closest to the adhesive e.g. a Carbon UD laminate. $\mathcal{G}_{ss}$ is decreased by approx. 5% for by adding the carbon UD buffer-layer with thickness $h_3/h_2 = 1.0$ to the Glass UD substrate ($h_1/h_2 = 1.0$). The largest deviation between Carbon UD isotropic and -orthotropic is approximately 7%, whereas the largest deviation between buffer-layers of Glass Biax and Carbon UD (isotropic) in Figure 7 is about 18%. Note, that the limit values indicated by arrows in Figure 7 are determined using the results of the bi-material FE model at $h_3/h_2 = 10$ in Figure 4.

The results in Figure 7 for Carbon UD can also be used to determine the best compromise between

buffer-layer thickness, -stiffness, and -price since too many Carbon UD layers would be costly in comparison with the constraining effect achieved. However, adding Carbon UD layers to an already stiff Glass UD laminate will only decrease $\mathcal{G}_{ss}$ by approx. up to 6-10% according to Figure 7. Instead, since the steady-state energy release rate scales linearly with the thickness of the adhesive layer, see equation 7, for the present case, it is more effective to decrease the energy release rate by decreasing the thickness of the adhesive layer.

7. Discussions

The implications and effects of the buffer-layer are discussed. In order to design a reliable adhesive joint, specific requirements for the properties of the buffer-layer must be set. If the tunneling crack initially confined in the adhesive, shown in Figure 8 (A), extends through the buffer-layer (Figure 8 (B)) then the energy release rate of the tunneling crack becomes higher since both the thickness- and the stiffness of the cracked layer increase (if $E_3 > E_2$). Thus, cracking through the buffer-layer increases the steady-state energy release rate of the tunneling crack dramatically. Therefore, the strength and fracture toughness of the buffer-layer must be sufficiently high to avoid cracking during the tunneling crack propagation across the bondline. Fortunately, laminates used in wind turbine blades have both higher stiffness and -strength than the typical structural adhesives used in wind turbine blades. Models for crack penetration of interlayers are available in the literature [18, 19, 20]; they can be used to set the requirements for the additional material properties of the buffer-layer. If the buffer-layer is a composite material with long aligned fibres, then it will be unlikely that a crack penetrates through the buffer-layer as a sharp crack. Instead, the tunneling crack will more likely cause damage to a larger zone and initiate splitting and delaminations of the laminates.

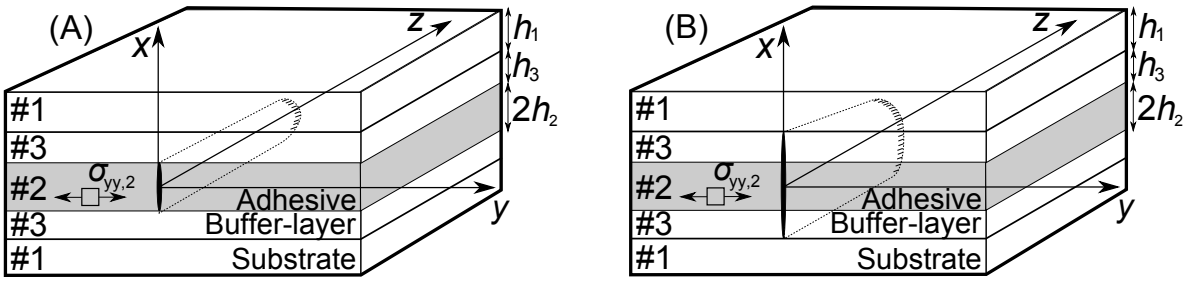

Figure 8: (A) Tunneling crack confined in the adhesive layer. (B) Tunneling crack extended through the buffer-layer.

The load required to propagate a tunneling crack is lower than the load to initiate a tunneling crack from a small void in the adhesive [2]. Thus, the use of the tunneling models as design criteria for bondlines containing voids (no real sharp cracks) is regarded as being conservative. Furthermore, if a tunneling crack initiates at a free edge then the tunneling crack must reach a certain length (dependent

on elastic mismatch) to become steady-state [7]. The energy release rate increases with crack length until the steady-state value is attained [2], which is another reason why the steady-state tunneling crack models are conservative.

For future work, the tri-material model in the present study may be extended to include the effect of adhesive-laminate debonding for both static and cyclic loadings [5, 6, 4] and extended to include multiple cracking [2, 21].

8. Conclusions

Generally, it was found favourable to embed a buffer-layer near the adhesive with controllable thickness- and stiffness properties in order to improve the joint design against the propagation of tunneling cracks. The results from the tri-material FE model showed that it was desirable to increase the thickness of the buffer-layer if the stiffness of the buffer-layer is higher than the "point of intersection" in Figure 6. In any case, it was advantageous to increase the stiffness of the buffer-layer in order to decrease the energy release rate of the tunneling crack.

For blade relevant materials, the effect of material orthotropy on the steady-state energy release rate was found to be relatively small (2-7%). Similarly, the effect of using a Carbon UD laminate as buffer-layer was relatively small (6-10%) since the stiffness of the original Glass UD laminate was already high. Instead, it is proposed to reduce the thickness of the adhesive layer in the wind turbine blade joint.

Acknowledgements

This research was primarily supported by grant no. 4135-00010B from Innovation Fund Denmark. This research was also supported by the Danish Centre for Composite Structure and Materials for Wind Turbines (DCCSM), grant no. 0603-00301B, from Innovation Fund Denmark.

Appendix A. Additional design curves from tri-material FE model

Additional design curves determined by the tri-material FE model are presented in Figure A.9 and Figure A.10. From these curves the transition at the "point of intersection" is investigated further i.e. for the energy release rate increasing with buffer-layer thickness to the energy release rate decreasing with buffer-layer thickness. This transition is difficult to identify from Figure A.9. Therefore, the design curves in Figure A.9 for $-0.5 < \alpha_{32} < 0.0$ are magnified and presented individually in Figure A.10. In Figure A.10, it is seen that the shape of the curve is very dependent on the magnitude of α_{32}. A peak is identified in Figure A.10 (B-G). The peak is reduced with increasing α_{32} (closer to zero). In

Figure A.10 (H-I) the peak vanish and for increasing h_1/h_2, a continuous decreasing trend is attained. It is of interest that a peak in Figure A.10 (A-G) exists since it is typically desired to minimise or maximise the energy release rate dependent on the application.

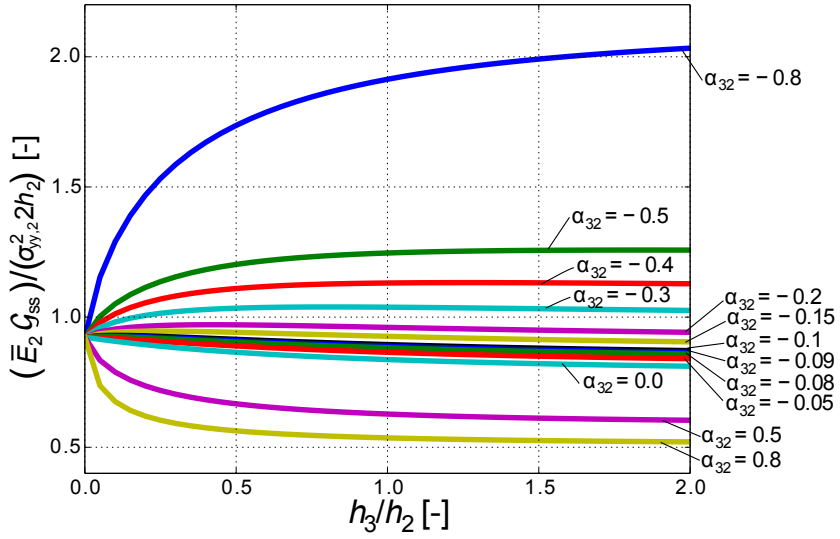

Figure A.9: Steady-state energy release rate results from a tri-material FE model with selected parameters fixed: $\beta_{i2} = \alpha_{i2}/4$, $h_1/h_2 = 1.0$, and substrate stiffness mismatch of: $\alpha_{12} = 0.0$.

References

[1] J. Z. Hansen, The effects of fibre architecture on fatigue life-time of composite materials, Ph.D. thesis, Technical University of Denmark. Dept. of Wind Energy, (2013).

[2] S. Ho, Z. Suo, Tunneling cracks in constrained layers, J. Appl. Mech 60 (1993) 890–894.

[3] Z. Suo, Failure of brittle adhesive joints, Appl. Mech 43 (5) (1990) 275–279.

[4] K. Chan, M. He, J. Hutchinson, Cracking and stress redistribution in ceramic layered composites, Materials Science and Engineering A167 (1993) 57–64.

[5] A. S. J. Suiker, N. A. Fleck, Crack tunneling and plane-strain delamination in layered solids, International Journal of Fracture 125 (1) (2004) 1–32. doi:10.1023/B:FRAC.0000021064.52949.e2.

[6] A. S. J. Suiker, N. A. Fleck, Modelling of fatigue crack tunneling and delamination in layered composites, Composites Part A: Applied Science and Manufacturing 37 (10) (2006) 1722–1733. doi:10.1016/j.compositesa.2005.09.006.

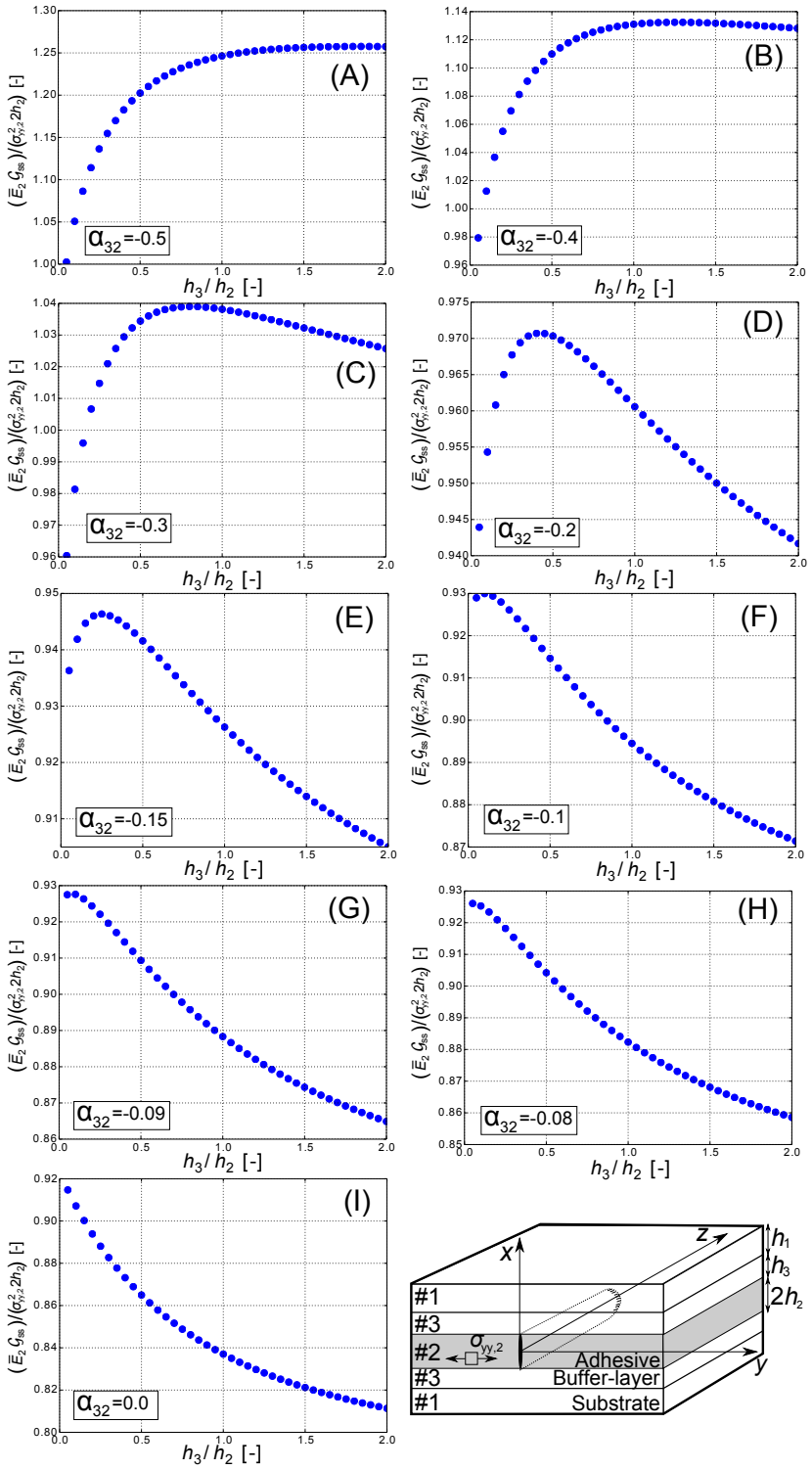

Figure A.10: Steady-state energy release rate results from a tri-material FE model with selected parameters fixed: $\beta_{i2} = \alpha_{i2}/4$, $h_1/h_2 = 1.0$, and substrate-adhesive stiffness mismatch of: $\alpha_{12} = 0.0$.

[7] J. Andersons, P. H. M. Timmermans, J. Modniks, Mechanics of tunnelling cracks in trilayer elastic materials in tension, International Journal of Fracture 148 (3) (2008) 233–241. doi:10.1007/s10704-008-9197-3.

[8] T. Nakamura, S. M. Kamath, Three-dimensional effects in thin film fracture mechanics, Mechanics of Materials 13 (1) (1992) 67–77. doi:10.1016/0167-6636(92)90037-E.

[9] J. M. Ambrico, M. R. Begley, The role of initial flaw size, elastic compliance and plasticity in channel cracking of thin films, Thin Solid Films 419 (2002) 144–153. doi:10.1016/S0040-6090(02)00718-6.

[10] T. Yang, Y. Liu, J. Wang, A study of the propagation of an embedded crack in a composite laminate of finite thickness, Composite Structures 59 (4) (2003) 473–479. doi:10.1016/S0263-8223(02)00284-2.

[11] H. Beom, X. Zhuo, C. Cui, Tunneling cracks in the adhesive layer of an orthotropic sandwich structure, International Journal of Engineering Science 63 (2013) 40–51. doi:10.1016/j.ijengsci.2012.11.001.

[12] Z. Suo, G. Bao, B. Fan, T. Wang, Orthotropy rescaling and implications for fracture in composites, Int. J. Solid Structures 28 (2) (1991) 235–248.

[13] T. Y. Tsui, A. J. McKerrow, J. J. Vlassak, Constraint effects on thin film channel cracking behavior, Journal of Materials Research 20 (2005) 2266–2273. doi:10.1557/jmr.2005.0317.

[14] J. Dundurs, Edge-bonded dissimilar orthogonal elastic wedges under normal and shear loading, Journal of Applied Mechanics 36 (3) (1969) 650–652.

[15] J. Parmigiani, M. Thouless, The effects of cohesive strength and toughness on mixed-mode delamination of beam-like geometries, Engineering Fracture Mechanics 74 (17) (2007) 2675–2699. doi:10.1016/j.engfracmech.2007.02.005.

[16] M. Leong, L. C. T. Overgaard, O. T. Thomsen, E. Lund, I. M. Daniel, Investigation of failure mechanisms in GFRP sandwich structures with face sheet wrinkle defects used for wind turbine blades, Composite Structures 94 (2) (2012) 768–778. doi:10.1016/j.compstruct.2011.09.012.

[17] L. P. Mikkelsen, A simplified model predicting the weight of the load carrying beam in a wind turbine blade, IOP Conference Series: Materials Science and Engineering 139 (2016) 1–8. doi:10.1088/1757-899X/139/1/012038.

[18] M. Y. He, J. W. Hutchinson, Crack deflection at an interface between dissimilar elastic materials, Int. J. Solid Structures 25 (9) (1989) 1053–1067.

[19] M. Y. He, A. G. Evans, Crack deflection at an interface between dissimilar elastic materials: Role of residual stresses, Int. J. Solids Structures 31 (1994) 3443.

[20] J. Parmigiani, M. Thouless, The roles of toughness and cohesive strength on crack deflection at interfaces, Journal of the Mechanics and Physics of Solids 54 (2) (2006) 266–287. doi:10.1016/j.jmps.2005.09.002.

[21] J. W. Hutchinson, Z. Suo, Mixed mode cracking in layered materials, Advances in applied mechanics 29 (1992) 63.